Optimization and Engineering
https://doi.org/10.1007/s11081-021-09678-0

RESEARCH ARTICLE

Reconstruction analysis of honeybee colony collapse disorder modeling

Atanas Z. Atanasov[1] · **Slavi G. Georgiev**[1] · **Lubin G. Vulkov**[1]

Received: 12 March 2021 / Revised: 12 August 2021 / Accepted: 13 August 2021

Abstract
The honeybee has a significant impact on industry and nature. In recent years, a mysterious disease make honeybees die, often losses reach 80–100% of the apiaries. The causal syndrome of such massive die-off is called Colony Collapse Disorder. The model adopted in the paper is constituted by a system of three ordinary differential equations that account for the change in time of the population size of the hive bees, forage workers and infected foragers. It models the condition as a contagion, transmitted by both bee-to-bee and bee-to-plant interaction. What is more, it supports both healthy and unhealthy population dynamics. We solve a parameter identification inverse problem to reconstruct the values, which are directly unobservable but vital in honeybee management. We apply an adjoint equation optimization approach to solve this inverse problem. Numerical analysis confirms the results obtained theoretically.

Keywords Honeybee population dynamics · Colony collapse disorder · Allee effect · Parameter identification · Adjoint equation optimization method

1 Introduction

The honeybee *Apis mellifera* plays a crucial role in both environmental balance and economy. Although it might seem odd at first glance, but the bee is looked at as one of the primary natural pollinators. Their contribution to pollination is evaluated to

✉ Slavi G. Georgiev
sggeorgiev@uni-ruse.bg

Atanas Z. Atanasov
aatanasov@uni-ruse.bg

Lubin G. Vulkov
lvalkov@uni-ruse.bg

[1] University of Ruse, 8 Studentska Str., 7017 Ruse, Bulgaria

Published online: 28 August 2021

exceed the value of honey products and its derivatives between 10 and 20 times. What is more, at the beginning of the millennium, the bee pollination activity is estimated to about $ 15 billion per year in US agriculture (Oldroyd 2007). Albert Einstein said that mankind would survive four years after the extinction of the bees. There would be no crops without pollination, thus animals will die of hunger—and the people with them.

Honeybee losses have happened many times at many places. There exist records for such events in the past century (Finley et al. 1996; Silver 1907), but the massive loss from the winter of 2006–2007 (Fact Sheet 2015) had some unique traits which have not been met before. There were beekeepers who suffered 80%, 90% and even 100% losses of their apiaries and it was not an isolated case since it was observed in Europe, Asia, America and other places (van der Zee et al. 2012). The first and most specific sign is the absence of adult bees in and around the hive. Such conditions have been recorded previously (Kulincevic et al. 1982), but there are other characteristic marks which caused the phenomenon to be named 'Colony Collapse Disorder' (CCD). Such an event happened repeatedly in recent years and could be described in general by its three distinctive features: (1) a massive loss of adult bees from colonies while no carcasses are present near the hive; (2) the availability of the queen and the capped brood; (3) the abandoned food supply, which is not robbed by scavenging species for an extended period of time. What is more, it is sometimes claimed that (4) during the colony collapse, *Varroa* mite and *Nosema* populations are not at levels known to cause a typical population decline (vanEngelsdorp et al. 2009). Moreover, the remaining bees are unwilling to use food provision provided by the beekeeper (Ellis et al. 2010).

The fact all researchers agree on is that it is not a single agent that causes CCD, but it is a complex of reasons. Unfortunately, so far there is still no consensus on the factors that lead to CCD. It is believed to be either a contagious disease or to result from exposure to a common risk factor (vanEngelsdorp et al. 2009). In this source a descriptive epizootiological study is conducted and many quantitative variables are studied. It is found that only the fittest honeybees remain in the CCD hives, because they appear to be more symmetrical than their counterparts in the «healthy» hives. Another interesting fact is that the latter might have developed tolerance to certain stressors, which possibly protects them. Nevertheless, the CCD colonies were found to be co-infected with a greater number of pathogens than the control ones, implying either greater pathogen exposure or reduced defenses in CCD bees.

A short list of possible hypotheses is presented in Ellis et al. (2010), including viruses, poor nutrition and management stress, while the author in Oldroyd (2007) researches different causative factors, from pesticides, genetically modified crops, various diseases and parasites, to narrow genetic base and cold brood (should the brood is raised in abnormal temperature, they become physically normal adult bees, but show deficiencies in learning and memory as well as they tend to get lost in the fields). They again conclude the CCD is caused by a combination of factors. Furthermore, in Cox-Foster et al. (2007) a metagenomic approach is employed to study the microflora in hives affected by CCD and to investigate the contribution of different pathogens in the colonies decline. It is found that the two *dicistroviruses*—Kashmir bee virus (KBV) and Israeli acute paralysis virus (IAPV) are present in almost

all of the CCD hives and in almost none of the control hives. The parasite *Nosema ceranae* is suggested to be the primary reason for a colony collapse in Spain (Paxton 2010). It is related to heavily affected colonies, despite the fact that it is denied to bring about CCD on its own.

In the next section the mathematical model is described. The inverse problem is formulated in Sect. 3 and the numerical methods for the direct and inverse problems are presented in Sects. 4 and 5, respectively. In addition, a basic qualitative analysis is provided is Sect. 4. Numerical experiments are given in Sect. 6, while the last section is dedicated to discussion and conclusion.

2 Model formulation

The mathematical models are vital to understand the underlying dynamics of a honeybee population. They could quantitatively describe the process in a colony thus simulate the development of the biological system and eventually help to design an escape way to prevent a colony collapse. In this section we are going to briefly review the existing models in the literature and to introduce the one we will use from now on.

To begin with, we will shed light on how a honeybee hive works. In a usual one, the bees can be classified into three distinct classes. The brood, which emerge from the queen's eggs, is raised by the young hive bees in a capped honeycomb compartment (Dornberger et al. 2012). When they mature out of the larvae stage, they become part of the hive worker class. Their responsibilities include nurturing the brood, building the combs of the hive, and also cleaning, repairing, ventilating and when needed—maintaining the temperature of the brood chamber in the hive (Winston 1991). They also take care of the food stores. After serving in the hive for between 7 and 21 days (Amdam and Omholt 2003), a hive bee matures and is recruited into the forager class (Winston 1991). A forager makes between 5 and 20 flights per day to pick up pollen and nectar from the plants. After serving as a forager bee for between 14 and 21 days during the foraging season, or up to 4 months in the winter, it eventually dies (Winston 1991). A healthy hive consists of between 50,000 and 80,000 honeybees during its peak foraging season (Dornberger et al. 2012).

A review of the existing dynamics models is done in Becher et al. (2013), where they are classified as colony, varroa, and foraging models. A link between the dynamics of a colony and of bee infection and diseases is incorporated in a model in Russel et al. (2013). The main finding in Russel et al. (2013); Torres et al. (2015) is the fact that the shortage of nutrition and the pheromone-driven social inhibition are the main causes of colony failure. A model taking into consideration the seasonal effects is developed in Switanek et al. (2017). Factors like infestation with parasites and viruses are considered in Ratti et al. (2017), while in Booton et al. (2017) it is explored the impact of the Allee effect on honeybees colony collapse via a simple compartment model. Such models that include the interaction of uninfected hive and forager bees, infected hive bees, virusfree mites and virus-infected mites are investigated in Bailey (2002); Ma et al. (2009).

In Khoury et al. (2011, 2013) the authors propose a model describing the honeybee colony population dynamics of two classes: the hive bees and the forage worker bees. Only the population of female bees is considered since the drones do not compose a significant portion of the colony and do not contribute to the hive and foraging work (Bagheri and Mirzaie 2019; Yıldız 2018). In the latter source, the author extends the model as introducing fractional-order derivatives of the rates of change of the bee classes population size, which activates the memory property and captures better the underlying dynamics. In Dornberger et al. (2012), a compartment model is suggested, where the honeybee population is constituted by three distinctive classes—hive bees, forager bees and infected forager bees, thus modeling the CCD as a contagious condition (Kribs-Zaleta and Mitchell 2014).

The model considers the development of a colony through an extended foraging season from early spring to late summer. The distinguishable sign of CCD is the massive loss of adult forage bees thus urging the hive workers to commence foraging, which strongly affects the colony and initiate the collapse (a hypothetical explanation of the strange absence of forage bees is that infested individuals evacuate themselves form their hives in attempt to prevent contamination of their fellows (Kralj and Fuchs 2006)). The model pays a special attention to this phenomenon.

The population size of the *hive* bees is denoted with H. Since the queen lays eggs at constant rate L, the maggots could mature into young hive bees at maximal rate L (Kribs-Zaleta and Mitchell 2014). Since the hive workers have a lot of responsibilities, their emergence is multiplied by a *saturation* function $\frac{H}{(H+\omega)}$, where ω represents the minimum number of bees needed to rear the brood in order for the hive to survive (Dornberger et al. 2012). From another point of view, the value of ω controls the rate of which the saturation function would reach 1 in case the number of hive workers becomes critically low. In Khoury et al. (2011, 2013) a similar saturation function is used, but they considered the whole population $H + F$ instead of only the hive bees H. Thus the *eclosion* rate is given by

$$\epsilon(H) = L\frac{H}{H+\omega}. \tag{1}$$

The population size of the *healthy forager* class is denoted with F, while the *infected forager* class population size—with I. After being hive bees (for a maximum of 3 weeks), they mature and join the forager class at rate γ. This process could be accelerated if the forager class is depleted and the hive needs more food (Kribs-Zaleta and Mitchell 2014). The maximal additional maturation rate is represented by α, and it is multiplied by another saturation function $\frac{\varphi}{(F+I+\varphi)}$, where $F + I$ is the total number of foragers, and φ is the total number of foragers, below which a maximal recruitment rate is accounted. In contrast, a maximum «healthy» recruitment rate is considered in Khoury et al. (2011, 2013), reduced by means of social inhibition when the forager class population becomes large. The *recruitment* rate is given by

$$\rho(F, I) = \alpha\frac{\varphi}{F+I+\varphi} + \gamma. \tag{2}$$

The model we follows assumes the disease transmission to be carried out via both bee-to-bee direct contact and contact with contaminated plants (Kribs-Zaleta and Mitchell 2014). The empirical analyses show that the foragers are most influenced by the CCD. What is more, the condition is spread through *mass action* between the foragers and the infected ones, while the foragers interact very little with the hive bees. Further assuming that the plants are not continuously occupied by the bees and the bees do not visit more plants than they are already visiting in case of plant density increase, then the *disease* rate is given by

$$\delta(I) = \beta \frac{I}{I+k}, \tag{3}$$

where β is the bee infection rate and $k = \frac{pc}{b}$, where p is the plant density, c is the rate at which the plants clear contamination, and b is the plant contamination rate.

Finally, the CCD model follows:

$$\frac{\mathrm{d}H}{\mathrm{d}t} = \epsilon(H) - H\rho(F,I) = L\frac{H}{H+\omega} - H\left(\alpha\frac{\varphi}{F+I+\varphi} + \gamma\right), \tag{4a}$$

$$\frac{\mathrm{d}F}{\mathrm{d}t} = H\rho(F,I) - \mu_1 F - F\delta(I) = H\left(\alpha\frac{\varphi}{F+I+\varphi} + \gamma\right) - \mu_1 F - \beta\frac{FI}{I+k}, \tag{4b}$$

$$\frac{\mathrm{d}I}{\mathrm{d}t} = F\delta(I) - \mu_2 I = \beta\frac{FI}{I+k} - \mu_2 I, \tag{4c}$$

where μ_1 is the natural forager mortality rate, the reciprocal of which denotes the average life longevity of a forager, and μ_2 is the death rate of infected foragers, its reciprocal representing the average time an infected bee remains a functional forager before leaving the hive or dying ($\mu_1 \leq \mu_2$). All rates are given in units time^{-1}, namely days^{-1}.

3 Inverse problem formulation

Inverse problems for systems of nonlinear differential equations like (4) arise in biology, epidemiology, ecology, etc. The inverse problems are ill-posed, meaning that a solution may not exist, may not be unique, and most importantly, may not continuously depend on the measurements. A class of numerical methods for solving ODE inverse problems are discussed in Abdulla and Poteau (2020). Another method is the 'collage method', see e. g. Kunze et al. (2004); it provides an excellent starting point for further optimization, in contrast to more traditional searching methods that require one first to select a good initial guess. A generalized collage method for solving inverse problems for boundary value problems is presented in Kunze et al. (2009), which is based on the Lax–Milgram representation theorem. An extended version of the Generalized Collage theorem is presented in Kunze et al. (2015) to cope with inverse problems for vector-valued Lax–Milgram systems. In Berenguer et al. (2016) a corresponding Galerkin

method is developed and a collage theorem is presented for a related inverse problem as a boundary value problems for linear impulse differential equations. An approach to solve inverse problems of ordinary differential equation using the Banach's fixed point theorem and Picard contraction mapping, borrowing from 'fractal-based' methods of approximation, is suggested in Kunze and Vrscay (1999). In the review Kunze et al. (2014) the contemporary fractal-based techniques and methods based on the Collage theorem are surveyed and the solutions to inverse problems for ordinary and partial differential equations are commented.

In this section we will define the inverse identification problem, or what and how we would be looking for. In the real world, the values of the parameters α, β, γ, μ_1 and μ_2 are typically unknown and their reconstruction plays a crucial role in the honeybee colony management. We employ the adjoint equation optimization method of Marchuk (1995); Marchuk et al. (1996).

The problem (4) is subjected to the following initial conditions:

$$H(t_0) = H^0, \quad F(t_0) = F^0, \quad I(t_0) = I^0, \tag{5}$$

where $\boldsymbol{p} = (p^1, p^2, p^3, p^4, p^5)$, $p^1 := \alpha$, $p^2 := \beta$, $p^3 := \gamma$, $p^4 := \mu_1$, $p^5 := \mu_2$ and

$$\boldsymbol{p} \in \mathbb{S}_{\text{adm}} = \left\{ \boldsymbol{p} \in \mathbb{R}^5 : \ 0 < p^i < P^i, \ i = 1, \ldots, 5 \right\}. \tag{6}$$

Henceforward all solutions $\{H(t;\boldsymbol{p}), F(t;\boldsymbol{p}), I(t;\boldsymbol{p})\}$, $\boldsymbol{p} \in \mathbb{S}_{\text{adm}}$ are defined on the interval $t_0 \le t \le T$. The admissible set $\mathbb{S}_{\text{adm}}$ follows the specification of the model (Kribs-Zaleta and Mitchell 2014) and the biology of the honey bees (Winston 1991). When the parameters α, β, γ, μ_1 and μ_2 are known, the problem (4), (5) is well-posed and it is called a *direct problem*.

Let us assume now that the coefficients p^i, $i = 1, \ldots, 5$ are unknown. We will solve the *inverse problem* for determination of the unknown parameter vector $\boldsymbol{p} = (\alpha, \beta, \gamma, \mu_1, \mu_2)$ at the measured values of the functions H, F, I:

$$H^{\text{obs}}(t_k;\boldsymbol{p}) = X_k, \ k = 1, \ldots, K_H, \tag{7}$$

$$F^{\text{obs}}(t_k;\boldsymbol{p}) = Y_k, \ k = 1, \ldots, K_F, \tag{8}$$

$$I^{\text{obs}}(t_k;\boldsymbol{p}) = Z_k, \ k = 1, \ldots, K_I. \tag{9}$$

The purpose of the inverse problem is to reconstruct these parameters from the observation data. The optimization method is a powerful tool for dealing with the ill-posed problems (Marchuk 1995; Marchuk et al. 1996).

4 Solution to the direct problem and a basic qualitative analysis

4.1 Numerical method

Now we will briefly show how to solve the direct problem (4)–(6). It is of a particular importance, because we need to solve the direct problem a couple of times in order to solve the inverse problem. For simplicity of the notation, in this section we assume that $K_H = K_F = K_I =: K$ and the points of measurements coincide for the three classes.

The following piecewise-uniform mesh is introduced:

$$\overline{\omega}_\tau = \left\{t_0,\ t_k = t_{k-1} + \tau_k J_k,\ t_K = T\right\} \text{ for } k = 1, \dots, K-1, \tag{10}$$

and the internal nodes between the observation times are defined as

$$t_k^j = t_{k-1} + j\tau_k,\ j = 1, \dots, J_k,$$

where $\forall k = 1, \dots, K$, t_k are the time instances at which observations are taken and τ_k are the time steps corresponding to $(t_{k-1}, t_k]$ (see Fig. 1 for an example, where $K = 4$).

For solving the initial problem (4), (5) we will employ an explicit Runge–Kutta method, associated with a fourth order accuracy. It is a standard and widely used approach for a non-stiff system of ODEs.

Let us write the system (4) in the form

$$\frac{\mathrm{d}\boldsymbol{R}}{\mathrm{d}t} = \boldsymbol{G}\big(t, \boldsymbol{R}(t)\big),$$

where $\boldsymbol{R} = (H, F, I)^\top$ and the initial condition (5) $\boldsymbol{R}_0 = \boldsymbol{R}(t_0)$ is given. The solution is presented in Algorithm 1.

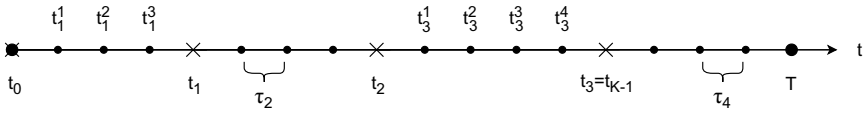

Fig. 1 Mesh ω_τ (10)

Algorithm 1 RK4

for $k = 1, \ldots, K$ **do**
  for $j = 0, \ldots, J_k - 1$ **do**
    Let $t := t_k^j$, $\hat{t} := t_k^{j+1}$, $\boldsymbol{R} := \boldsymbol{R}(t)$, $\hat{\boldsymbol{R}} := \boldsymbol{R}(\hat{t})$. Then $\hat{\boldsymbol{R}}$ is calculated as

$$\hat{\boldsymbol{R}} = \boldsymbol{R} + \frac{1}{6}\left(\boldsymbol{k}_1 + 2\boldsymbol{k}_2 + 2\boldsymbol{k}_3 + \boldsymbol{k}_4\right),$$

  where

$$\boldsymbol{k}_1 = \tau_k \boldsymbol{G}(t,\ \boldsymbol{R}), \quad \boldsymbol{k}_2 = \tau_k \boldsymbol{G}\left(t + \frac{\tau_k}{2},\ \boldsymbol{R} + \frac{\boldsymbol{k}_1}{2}\right),$$
$$\boldsymbol{k}_3 = \tau_k \boldsymbol{G}\left(t + \frac{\tau_k}{2},\ \boldsymbol{R} + \frac{\boldsymbol{k}_2}{2}\right), \quad \boldsymbol{k}_4 = \tau_k \boldsymbol{G}(\hat{t},\ \boldsymbol{R} + \boldsymbol{k}_3).$$

  end for
end for

4.2 A qualitative analysis

In this subsection we introduce some basic notions and definitions that will be used in our computational simulations performed on the base of (the solution to) the inverse problem.

4.2.1 Equilibria analysis

First, following Kribs-Zaleta and Mitchell (2014), we introduce some results from the equilibria analysis of the model (4a)–(4c). In Kribs-Zaleta and Mitchell (2014) a thorough equilibria analysis is performed. We will summarize the relevant information. There are six equilibria of the system (4), five of which are biologically relevant. First to mention is the *extinction* equilibrium

$$H = 0,\ F = 0,\ I = 0,$$

which always exists and is stable provided that $L < \omega(\alpha + \gamma)$.

Furthermore, there are two different *disease-free* equilibria, which exist if

$$\alpha\omega > \mu_1\varphi \quad \text{and} \quad 2\sqrt{\alpha\mu_1\varphi\omega} - \mu_1\varphi \le L - \gamma\omega.$$

It is the larger disease-free equilibrium that requires satisfying the inequalities. The smaller one exists if they are met, or if

$$L < \omega(\alpha + \gamma).$$

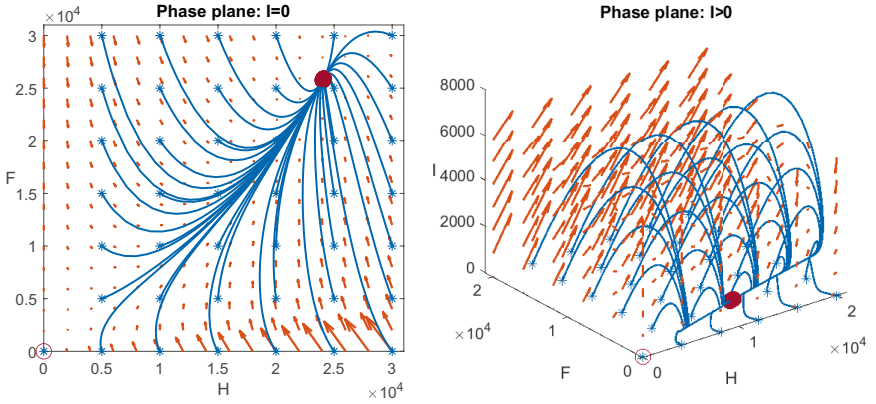

Fig. 2 Phase plane diagram of the solution in the case $I = 0$ (left) and $I > 0$ (right)

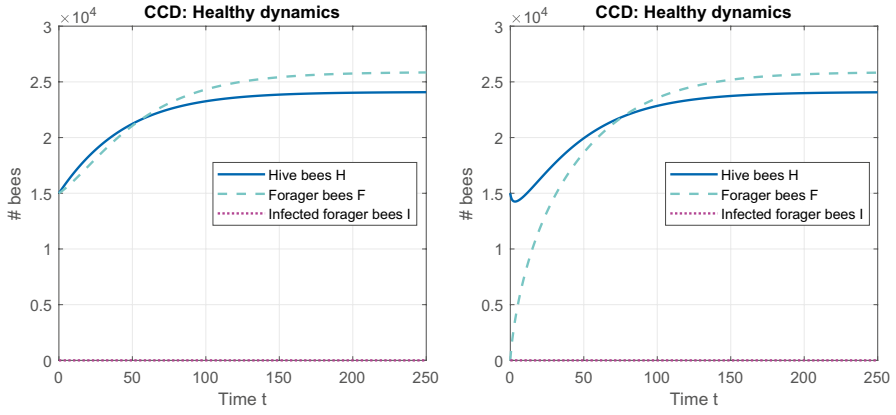

Fig. 3 Healthy dynamics: $F^0 = 15{,}000$ (left) and $F^0 = 0$ (right)

They can exist at the same time (Dornberger et al. 2012). While the smaller disease-free equilibrium is always unstable, the larger one is stable when the basic reproduction number is below one. We will discuss it shortly.

There are two *endemic* equilibria as well. They exist under complicated conditions, please refer to Table 1 in Kribs-Zaleta and Mitchell (2014). The larger endemic equilibrium is always stable, while the smaller one is always unstable.

To investigate the population dynamics of the hive, regarding its biological processes, the population is explored for 250 days. To simulate particular cases, we assume that $L < \omega(\alpha + \gamma)$ is fulfilled. First we consider the disease-free case, i. e. when $I^0 = 0$. The respective phase plane diagram is presented on Fig. 2 (left), compare with Fig. 3.

The blue curves follow concrete solutions development and the stars denote the starting points. The filled circles show the equilibria states (simulated for one

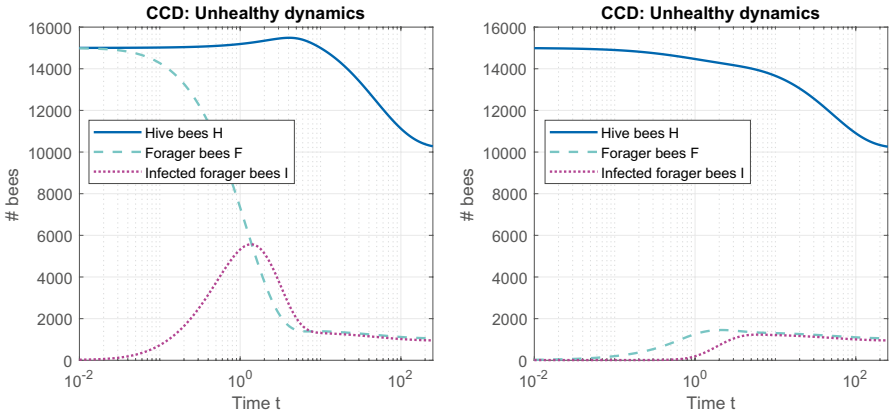

Fig. 4 Unhealthy dynamics: $F^0 = 15{,}000$ (left) and $F^0 = 0$ (right)

forage season), while the hollow circle denotes the extinction equilibrium. All the solutions (except in the extinction case) tend to the disease-free equilibrium, which is normal for a healthy colony.

It is also interesting when the unhealthy population dynamics is involved. The filled circles on Fig. 2 (right) designate the end points after one foraging season. All the solutions tend to an endemic equilibrium, which is characterized by low number of healthy foragers and comparable number of infected foragers. It could be observed on Fig. 4 as well.

Analyzing the equilibrium points $(H^\infty, F^\infty, I^\infty)$ and $(H^\infty, F^\infty, 0)$ is necessary because it allows the beekeepers to understand the continual death rate of the mites they must achieve in order to eliminate them. Knowing the percent of the mites continually dying out or being removed in a hive go to zero would aid in controlling the mite population and the longevity of the hive.

4.2.2 Basic reproduction number

In the theory of contagious disease modeling, the concept of the *basic reproduction number* $\mathcal{R}_0$ plays a central role since it measures the transmission potential of infectious diseases (Chowell and Brauer 2009). One of the fundamental results in the mathematical epidemiology is that there is a difference in the epidemic behaviour of the system depending on whether the basic reproduction number is less than one or more than one. It is a prominent example of the so called «threshold» behaviour.

If the system is closed, i. e. there are no vital dynamics involved, the situation is simple. If $\mathcal{R}_0 < 1$, the disease dies out, or if $\mathcal{R}_0 > 1$, the infection breaks out into epidemics. Unfortunately, this is not the case with the system (4) describing the honeybee population dynamics. The difference is in the latter case $\mathcal{R}_0 > 1$, in which there is also a possibility for the disease to persist in the population. Concerning a honeybee colony, when there are no infection, the system approaches its disease-free equilibrium, which is asymptotically stable. In case the contagion sticks with the

hive, the disease-free equilibrium is unstable and the population is in an endemic equilibrium, which is usually stable. Of course, if the colony is strongly influenced by the disease, it goes into the extinction equilibrium.

There is a change in the equilibrium behaviour (or *bifurcation*) at $\mathcal{R}_0 = 1$, but the equilibrium infective population size depends continuously on $\mathcal{R}_0$. This phenomenon is called a forward or transcritical bifurcation. However, with a backward bifurcation at $\mathcal{R}_0 = 1$, the equilibrium infective population size is zero for $\mathcal{R}_0 < 1$ but then jumps to a positive endemic equilibrium when $\mathcal{R}_0$ approaches 1. Another difference is that in case of a forward bifurcation at $\mathcal{R}_0 = 1$, for $\mathcal{R}_0 < 1$ the system would return to a disease-free equilibrium $I^\infty = 0$ if some infected individuals are introduced. On the contrary, if there is a backward bifurcation of $\mathcal{R}_0 = 1$ and enough infectives are introduced in the population to alter the initial state of the system above the unstable endemic equilibrium with $\mathcal{R}_0 < 1$, then the system would go to the stable endemic equilibrium, see e. g. Chowell and Brauer (2009) for further explanation.

The basic reproduction number is $\mathcal{R}_0$ is defined as the number of secondary infections caused by a single infective individual introduced into a wholly susceptible population over the course of the infection of this single infective (Chowell and Brauer 2009). In particular, our compartment model suggests infectives to populate only a single class (I). In this case, the basic reproduction number is calculated relatively easy. Let us consider again the infective dynamics (4c):

$$\frac{\mathrm{d}I}{\mathrm{d}t} = \beta \frac{FI}{I+k} - \mu_2 I \overset{!}{<} 0,$$

which is equivalent to

$$\frac{\beta F}{\mu_2 (I+k)} < 1.$$

It is found that $\mathcal{R}_0$ is defined only when the larger disease-free equilibrium exists (see Kribs-Zaleta and Mitchell (2014), Fig. 3). In this case, there is no infection, i. e. $I^\infty = 0$, thus the basic reproduction number reads

$$\mathcal{R}_0 = \frac{\beta F^\infty}{\mu_2 k}. \tag{11}$$

If $\mathcal{R}_0 > 1$, then one or both endemic equilibria exist and the disease persists within the colony. It is also possible that no endemic equilibrium exists and the colony goes into extinction because of CCD. When $\mathcal{R}_0 < 1$, if one disease-free equilibrium exists, it is always stable and the extinction equilibrium is unstable. If both disease-free equilibria exist, the larger one is always stable while the smaller one is unstable. As a consequence, if the initial condition is below the latter, the colony is attracted to the stable extinction equilibrium due to demographic failure (Dornberger et al. 2012). This is a manifestation of an *Allee effect*.

4.2.3 Allee effect

The Allee effect could be generally defined as a positive correlation between individual fitness and population size or density. The classical view of the population dynamics states that due to competition for resources, a population would experience a reduced overall growth rate at higher size or density and increased growth rate at lower size or density. It is shown, however, that the reverse holds true for low population size or density since individual may require assistance or protection by their mates in order to survive. Density-dependent effects could be either positive or negative and they greatly impact the population dynamics by modifying the species' population per capita growth rate (Usaini et al. 2017).

There are different characteristics after which an Allee effect could be classified. The component Allee effect is the positive relationship between any measurable component of the individual fitness and the population size or density. The demographic Allee effect is the positive relationship between the overall individual fitness and the population size or density. The presence of a component Allee effect does not necessarily lead to a demographic Allee effect, while the presence of a demographic Allee effect indicates the presence of at least one component Allee effect.

Furthermore, the Allee effect has a weak and a strong form. A population is said to exhibit a strong Allee effect when the growth rate is negative at low population size or density (Usaini et al. 2017). This directly implies the existence of a threshold below which the colony collapses to extinction. If the population growth rate is positive at low population size or density, the corresponding Allee effect is weak. In the latter case no critical thresholds exist.

Recently it has been studied how the mechanisms evoking an Allee effect influence the dynamics of a population at higher population size or density. It has been found that the combined impact of an infectious disease and a strong Allee effect could lead to an increase of the survival threshold, thus driving the population to inevitable extinction. The presence of a backward bifurcation involves the existence of a forward and a saddle-node bifurcations. When the two endemic equilibria merge and disappear, it is only the extinction attractor left. If the pathogenicity of the disease is very high, a second saddle-node bifurcation exists and is separate from the first one. In some cases, increasing $\mathcal{R}_0$ could be beneficial since it facilitates endemic persistence rather than extinction, see e. g. Usaini et al. (2017) for further detail.

Considering the honeybee population dynamics, there are two cases where an Allee effect operates. If $\mathcal{R}_0 < 1$ and both disease-free equilibria exist, an Allee effect emerges as it might repel the system from the smaller disease-free equilibrium and drive it to extinction, as we mentioned earlier. When $\mathcal{R}_0 > 1$, an Allee effect separates the larger endemic equilibrium from colony extinction, see again Fig. 3 and 4 in Kribs-Zaleta and Mitchell (2014) for a visualization.

5 Solution to the inverse problem

5.1 The adjoint equation optimization approach

Very often, the pointwise observation inverse problems are solved via the minimization of appropriate functionals, see e. g. Marchuk (1995), Marchuk et al. (1996)) and for an application (Atanasov et al. 2021). We will minimize the least-square functional

$$J(\boldsymbol{p}) = J(\alpha, \beta, \gamma, \mu_1, \mu_2) = J_H(\boldsymbol{p}) + J_F(\boldsymbol{p}) + J_I(\boldsymbol{p}), \tag{12}$$

where

$$J_H(\boldsymbol{p}) = \sum_{k=1}^{K_H} \left(H(t_k;\boldsymbol{p}) - X_k\right)^2,$$
$$J_F(\boldsymbol{p}) = \sum_{k=1}^{K_F} \left(F(t_k;\boldsymbol{p}) - Y_k\right)^2,$$
$$J_I(\boldsymbol{p}) = \sum_{k=1}^{K_I} \left(I(t_k;\boldsymbol{p}) - Z_k\right)^2.$$

The formulated inverse problem could be solved by gradient methods, see e. g. (Ma and Jiang 2007).

5.2 The gradient method

Theorem 1 *The gradient* $J'_{\boldsymbol{p}} \equiv (J'_\alpha, J'_\beta, J'_\gamma, J'_{\mu_1}, J'_{\mu_2})$ *of the functional* $J(\boldsymbol{p})$ *is given by*

$$\begin{aligned}
J'_\alpha(\boldsymbol{p}) &= \int_0^T H\frac{\varphi}{F+I+\varphi}(\phi_H - \phi_F)\mathrm{d}t,\\
J'_\beta(\boldsymbol{p}) &= \int_0^T \frac{FI}{I+k}(\phi_F - \phi_I)\mathrm{d}t,\\
J'_\gamma(\boldsymbol{p}) &= \int_0^T H(\phi_H - \phi_F)\mathrm{d}t,\\
J'_{\mu_1}(\boldsymbol{p}) &= \int_0^T F\phi_F\mathrm{d}t,\\
J'_{\mu_2}(\boldsymbol{p}) &= \int_0^T I\phi_I\mathrm{d}t,
\end{aligned} \tag{13}$$

where the functions $\phi_H = \phi_H(t)$, $\phi_F = \phi_F(t)$, $\phi_I = \phi_I(t)$ *are the unique solutions to the adjoint final-value problem*

$$
\begin{aligned}
&\frac{\mathrm{d}\phi_H}{\mathrm{d}t} = -L\frac{\omega}{(H+\omega)^2}\phi_H + \left(\alpha\frac{\varphi}{F+I+\varphi}+\gamma\right)(\phi_H-\phi_F) + 2\sum_{k=1}^{K_H}(H(t;\boldsymbol{p})-X(t))\delta(t-t_k),\\
&\frac{\mathrm{d}\phi_F}{\mathrm{d}t} = \frac{H\alpha\varphi}{(F+I+\varphi)^2}(\phi_F-\phi_H) + \mu_1\phi_F + \beta\frac{I}{I+k}(\phi_F-\phi_I) + 2\sum_{k=1}^{K_F}(F(t;\boldsymbol{p})-Y(t))\delta(t-t_k),\\
&\frac{\mathrm{d}\phi_I}{\mathrm{d}t} = \frac{H\alpha\varphi}{(F+I+\varphi)^2}(\phi_F-\phi_H) + \beta\frac{Fk}{(I+k)^2}(\phi_F-\phi_I) + \mu_2\phi_I + 2\sum_{k=1}^{K_I}(I(t;\boldsymbol{p})-Z(t))\delta(t-t_k),\\
&\phi_H(T)=0,\quad \phi_F(T)=0,\quad \phi_I(T)=0.
\end{aligned}
\tag{14}
$$

Proof We denote $\delta\boldsymbol{p}=(\delta\alpha,\delta\beta,\delta\gamma,\delta\mu_1,\delta\mu_2)$, $\delta\alpha=\varepsilon h_1$, $\delta\beta=\varepsilon h_2$, $\delta\gamma=\varepsilon h_3$, $\delta\mu_1=\varepsilon h_4$, $\delta\mu_2=\varepsilon h_5$ and $\delta H(t;\boldsymbol{p})=H(t;\boldsymbol{p}+\delta\boldsymbol{p})-H(t;\boldsymbol{p})$, $\delta F(t;\boldsymbol{p})=F(t;\boldsymbol{p}+\delta\boldsymbol{p})-F(t;\boldsymbol{p})$, $\delta I(t;\boldsymbol{p})=I(t;\boldsymbol{p}+\delta\boldsymbol{p})-I(t;\boldsymbol{p})$. Then we write the system (4) at $\boldsymbol{p}:=\boldsymbol{p}+\delta\boldsymbol{p}$ for the triplet $\{H(t;\boldsymbol{p}+\delta\boldsymbol{p}),F(t;\boldsymbol{p}+\delta\boldsymbol{p}),I(t;\boldsymbol{p}+\delta\boldsymbol{p})\}$ with initial data $\{H^0,F^0,I^0\}$. Next, we perform the differences between the corresponding equations to obtain a system for the tuple $\{\delta H(t;\boldsymbol{p}),\delta F(t;\boldsymbol{p}),\delta I(t;\boldsymbol{p})\}$ with zero initial conditions. After some algebra, we obtain:

$$
\begin{aligned}
\frac{\mathrm{d}}{\mathrm{d}t}\delta H = &\left(L\frac{\omega}{(H+\omega)^2}-\alpha\frac{\varphi}{F+I+\varphi}-\gamma\right)\delta H + \frac{H\alpha\varphi}{(F+I+\varphi)^2}\delta F + \frac{H\alpha\varphi}{(F+I+\varphi)^2}\delta I\\
&- H\frac{\varphi}{F+I+\varphi}\delta\alpha - H\delta\gamma + \mathcal{O}(\delta\cdot),
\end{aligned}
\tag{15}
$$

$$
\begin{aligned}
\frac{\mathrm{d}}{\mathrm{d}t}\delta F = &\left(\alpha\frac{\varphi}{F+I+\varphi}+\gamma\right)\delta H - \left(\frac{H\alpha\varphi}{(F+I+\varphi)^2}+\mu_1+\beta\frac{I}{I+k}\right)\delta F\\
&- \left(\frac{H\alpha\varphi}{(F+I+\varphi)^2}+\beta\frac{Fk}{(I+k)^2}\right)\delta I\\
&+ H\frac{\varphi}{F+I+\varphi}\delta\alpha - \frac{FI}{I+k}\delta\beta + H\delta\gamma - F\delta\mu_1 + \mathcal{O}(\delta\cdot),
\end{aligned}
\tag{16}
$$

$$
\frac{\mathrm{d}}{\mathrm{d}t}\delta I = \beta\frac{I}{I+k}\delta F + \left(\beta\frac{Fk}{(I+k)^2}-\mu_2\right)\delta I + \frac{FI}{I+k}\delta\beta - I\delta\mu_2 + \mathcal{O}(\delta\cdot). \tag{17}
$$

Let us find the increment of the functional $J(\boldsymbol{p})$ (12):

$$
\begin{aligned}
J(\boldsymbol{p}+\delta\boldsymbol{p})-J(\boldsymbol{p}) &= \sum_{k=1}^{K_H}(\delta H(t_k;\boldsymbol{p})+H(t_k;\boldsymbol{p})-X_k)^2-\sum_{k=1}^{K_H}(H(t_k;\boldsymbol{p})-X_k)^2\\
&+\sum_{k=1}^{K_F}(\delta F(t_k;\boldsymbol{p})+F(t_k;\boldsymbol{p})-Y_k)^2-\sum_{k=1}^{K_F}(F(t_k;\boldsymbol{p})-X_k)^2\\
&+\sum_{k=1}^{K_I}(\delta I(t_k;\boldsymbol{p})+I(t_k;\boldsymbol{p})-Z_k)^2\\
&-\sum_{k=1}^{K_I}(I(t_k;\boldsymbol{p})-Z_k)^2=\sum_{k=1}^{K_H}\delta H(t_k;\boldsymbol{p})\big(\delta H(t_k;\boldsymbol{p})+2(H(t_k;\boldsymbol{p})-X_k)\big)\\
&+\sum_{k=1}^{K_F}\delta F(t_k;\boldsymbol{p})\big(\delta F(t_k;\boldsymbol{p})+2(F(t_k;\boldsymbol{p})-Y_k)\big)\\
&+\sum_{k=1}^{K_I}\delta I(t_k;\boldsymbol{p})\big(\delta I(t_k;\boldsymbol{p})+2(I(t_k;\boldsymbol{p})-Z_k)\big)\\
&=2\sum_{k=1}^{K_H}\delta H(t_k;\boldsymbol{p})(H(t_k;\boldsymbol{p})-X_k)+2\sum_{k=1}^{K_F}\delta F(t_k;\boldsymbol{p})(F(t_k;\boldsymbol{p})-Y_k)\\
&+2\sum_{k=1}^{K_I}\delta I(t_k;\boldsymbol{p})(I(t_k;\boldsymbol{p})-Z_k)\\
&+\sum_{k=1}^{K_H}(\delta H(t_k;\boldsymbol{p}))^2+\sum_{k=1}^{K_F}(\delta F(t_k;\boldsymbol{p}))^2+\sum_{k=1}^{K_I}(\delta I(t_k;\boldsymbol{p}))^2.
\end{aligned}
$$

Since $\delta H(t_k;\boldsymbol{p})=\mathcal{O}(\varepsilon)$, $\delta F(t_k;\boldsymbol{p})=\mathcal{O}(\varepsilon)$, $\delta I(t_k;\boldsymbol{p})=\mathcal{O}(\varepsilon)$ we can write the increment of the functional $J(\boldsymbol{p})$ is integral form as

$$
\begin{aligned}
J(\boldsymbol{p}+\delta\boldsymbol{p})-J(\boldsymbol{p}) =& 2\sum_{k=1}^{K_H}\int_0^T\delta H(t;\boldsymbol{p})(H(t;\boldsymbol{p})-X(t))\delta(t-t_k)\mathrm{d}t\\
&+2\sum_{k=1}^{K_F}\int_0^T\delta F(t;\boldsymbol{p})(F(t;\boldsymbol{p})-Y(t))\delta(t-t_k)\mathrm{d}t\\
&+2\sum_{k=1}^{K_I}\int_0^T\delta I(t;\boldsymbol{p})(I(t;\boldsymbol{p})-Z(t))\delta(t-t_k)\mathrm{d}t+\mathcal{O}(\varepsilon).
\end{aligned}
\tag{18}
$$

Following the main idea of the adjoint equation method, see e. g. Marchuk (1995), we multiply the equation (15) by a smooth function $\phi_H(t)$ such that $\phi_H(T)=0$, equation (16) by a function $\phi_F(t)$ such that $\phi_F(T)=0$ and equation (17) by a function $\phi_I(t)$, $\phi_I(T)=0$ (later these functions would be fully identified). We integrate both sides of the results from 0 to T and add them together:

$$
\begin{aligned}
&\int_0^T \left(\phi_H \frac{\mathrm{d}}{\mathrm{d}t}\delta H + \phi_F \frac{\mathrm{d}}{\mathrm{d}t}\delta F + \phi_I \frac{\mathrm{d}}{\mathrm{d}t}\delta I\right)\mathrm{d}t \\
&= \int_0^T \phi_H \left(L\frac{\omega}{(H+\omega)^2} - \alpha\frac{\varphi}{F+I+\varphi} - \gamma\right)\delta H \mathrm{d}t \\
&\quad + \int_0^T \phi_H \frac{H\alpha\varphi}{(F+I+\varphi)^2}\delta F \mathrm{d}t + \int_0^T \phi_H \frac{H\alpha\varphi}{(F+I+\varphi)^2}\delta I \mathrm{d}t \\
&\quad - \int_0^T \phi_H H \frac{\varphi}{F+I+\varphi}\delta\alpha \mathrm{d}t - \int_0^T \phi_H H\delta\gamma \mathrm{d}t \\
&\quad + \int_0^T \phi_F \left(\alpha\frac{\varphi}{F+I+\varphi} + \gamma\right)\delta H \mathrm{d}t - \int_0^T \phi_F \left(\frac{H\alpha\varphi}{(F+I+\varphi)^2} + \mu_1 + \beta\frac{I}{I+k}\right)\delta F \mathrm{d}t \\
&\quad - \int_0^T \phi_F \left(\frac{H\alpha\varphi}{(F+I+\varphi)^2} + \beta\frac{Fk}{(I+k)^2}\right)\delta I \mathrm{d}t + \int_0^T \phi_F H \frac{\varphi}{F+I+\varphi}\delta\alpha \mathrm{d}t \\
&\quad - \int_0^T \phi_F \frac{FI}{I+k}\delta\beta \mathrm{d}t + \int_0^T \phi_F H\delta\gamma \mathrm{d}t - \int_0^T \phi_F F\delta\mu_1 \mathrm{d}t + \int_0^T \phi_I \beta\frac{I}{I+k}\delta F \mathrm{d}t \\
&\quad + \int_0^T \phi_I \left(\beta\frac{Fk}{(I+k)^2} - \mu_2\right)\delta I \mathrm{d}t + \int_0^T \phi_I \frac{FI}{I+k}\delta\beta \mathrm{d}t - \int_0^T \phi_I I\delta\mu_2 \mathrm{d}t + \mathcal{O}(\varepsilon).
\end{aligned}
$$

Integrating by parts the left-hand side and using the fact that $\phi_H(T) = 0$, $\delta H(0) = 0$, $\phi_F(T) = 0$, $\delta F(0) = 0$, $\phi_I(T) = 0$, $\delta I(0) = 0$, we obtain:

$$
\int_0^T \left(\phi_H \frac{\mathrm{d}}{\mathrm{d}t}\delta H + \phi_F \frac{\mathrm{d}}{\mathrm{d}t}\delta F + \phi_I \frac{\mathrm{d}}{\mathrm{d}t}\delta I\right)\mathrm{d}t = -\int_0^T \delta H \frac{\mathrm{d}\phi_H}{\mathrm{d}t}\mathrm{d}t - \int_0^T \delta F \frac{\mathrm{d}\phi_F}{\mathrm{d}t}\mathrm{d}t - \int_0^T \delta I \frac{\mathrm{d}\phi_I}{\mathrm{d}t}\mathrm{d}t. \tag{19}
$$

Then, placing the expressions for $\frac{\mathrm{d}\phi_H}{\mathrm{d}t}$, $\frac{\mathrm{d}\phi_F}{\mathrm{d}t}$, $\frac{\mathrm{d}\phi_I}{\mathrm{d}t}$ from (14) in (19) and using (18), after some algebraic manipulations we find

$$
\begin{aligned}
&J(\boldsymbol{p}+\delta\boldsymbol{p}) - J(\boldsymbol{p}) \equiv J(\alpha+\varepsilon h_1, \beta+\varepsilon h_2, \gamma+\varepsilon h_3, \mu_1+\varepsilon h_4, \mu_2+\varepsilon h_5) - J(\alpha,\beta,\gamma,\mu_1,\mu_2) \\
&\quad = \delta\alpha \int_0^T \phi_H H \frac{\varphi}{F+I+\varphi}\mathrm{d}t + \delta\gamma \int_0^T \phi_H H \mathrm{d}t - \delta\alpha \int_0^T \phi_F H \frac{\varphi}{F+I+\varphi}\mathrm{d}t \\
&\quad + \delta\beta \int 0^T \phi_F \frac{FI}{I+k}\mathrm{d}t - \delta\gamma\phi_F H \mathrm{d}t + \delta\mu_1 \int_0^T \phi_F F \mathrm{d}t \\
&\quad - \delta\beta \int_0^T \phi_I \frac{FI}{I+k}\mathrm{d}t + \delta\mu_2 \int_0^T \phi_I I \mathrm{d}t + \mathcal{O}(\varepsilon).
\end{aligned}
$$

Now, taking $h_2 = h_3 = h_4 = h_5 = 0$, dividing both sides of the latter equality by εh_1 and passing to the limit $\varepsilon \to 0$, we obtain the formula for J'_α in (13). In the same manner one can check the validity of the other four formulae in (13). □

Using the main property of the Dirac-delta function $\int_0^T \mathfrak{f}(t)\delta(t-t_k)\mathrm{d}t = \mathfrak{f}(t_k)$, $t_k \in (0,T)$, where $\mathfrak{f}(t)$ is a continuous function, we could rewrite the problem (14) in the equivalent form

$$
\begin{aligned}
&\frac{\mathrm{d}\phi_H}{\mathrm{d}t} = -L\frac{\omega}{(H+\omega)^2}\phi_H + \left(\alpha\frac{\varphi}{F+I+\varphi}+\gamma\right)(\phi_H-\phi_F), \quad t\in(0,T),\ t\neq t_k,\ k=1,\dots,K_H,\\
&\frac{\mathrm{d}\phi_F}{\mathrm{d}t} = \frac{H\alpha\varphi}{(F+I+\varphi)^2}(\phi_F-\phi_H)+\mu_1\phi_F+\beta\frac{I}{I+k}(\phi_F-\phi_I), \quad t\in(0,T),\ t\neq t_k,\ k=1,\dots,K_F,\\
&\frac{\mathrm{d}\phi_I}{\mathrm{d}t} = \frac{H\alpha\varphi}{(F+I+\varphi)^2}(\phi_F-\phi_H)+\beta\frac{Fk}{(I+k)^2}(\phi_F-\phi_I)+\mu_2\phi_I, \quad t\in(0,T),\ t\neq t_k,\ k=1,\dots,K_I,\\
&\left[\phi_H\right]_{t=t_k} = 2\big(H(t_k;\boldsymbol{p})-X_k\big), \quad k=1,\dots,K_H,\\
&\left[\phi_F\right]_{t=t_k} = 2\big(F(t_k;\boldsymbol{p})-Y_k\big), \quad k=1,\dots,K_F,\\
&\left[\phi_I\right]_{t=t_k} = 2\big(I(t_k;\boldsymbol{p})-Z_k\big), \quad k=1,\dots,K_I,\\
&\phi_H(T)=0, \quad \phi_F(T)=0, \quad \phi_I(T)=0,
\end{aligned}
\tag{20}
$$

and solve it instead of (14).

5.3 Algorithm

We now present a numerical algorithm for solving the nonlinear optimization problem (7)–(9), (12). It is a conjugate gradient method, seeking for the minimizer $\check{\boldsymbol{p}}$, which is detailed in Algorithm 2.

Algorithm 2 Adjoint Equation Optimization Method

Initialize $\boldsymbol{p}_0 \in \mathrm{S}_{\mathrm{adm}}$ and $l=-1$.
repeat
$l := l+1$
Solve the direct problem (4)-(6) at the current value $\boldsymbol{p}_l$ by the method described in Sect. 4. Then, define

$$H(t_k;\boldsymbol{p}_l)=X_k,\ k=1,\dots,K_H;\ F(t_k;\boldsymbol{p}_l)=Y_k,\ k=1,\dots,K_F;\ I(t_k;\boldsymbol{p}_l)=Z_k,\ k=1,\dots,K_I$$

Solve the adjoint problem (14) or (20)
Compute $J'(\boldsymbol{p}_l)$ by formulae (13)
Using a conjugate gradient method, define the optimization parameter $\boldsymbol{r}_l > 0$ and compute the new parameter value $\boldsymbol{p}_{l+1}$ by formula

$$\boldsymbol{p}_{l+1} = \boldsymbol{p}_l - \boldsymbol{r}_l J'(\boldsymbol{p}_l), \quad \boldsymbol{r}_l > 0,\ \boldsymbol{r}_l \in \mathbb{R}^+_5 \tag{21}$$

until $\|\triangle\boldsymbol{p}_l\| := \|\boldsymbol{p}_{l+1}-\boldsymbol{p}_l\| < \varepsilon_{\boldsymbol{p}}$
Set $\check{\boldsymbol{p}} := \boldsymbol{p}_{l+1}$

In application, the threshold $\varepsilon_{\boldsymbol{p}}$ is chosen according to the practical needs and the values of the descent parameter $\boldsymbol{r}_l$ are chosen empirically, please see the next section for further details.

6 Numerical examples

We now present numerical tests with the proposed method for the parameter reconstruction of CCD from *limited* observation data. All computations are performed in MATLAB® environment.

In order to test the accuracy and robustness of the proposed method, we first investigate an artificially constructed example. In it, we choose the values of the coefficients $\alpha, \beta, \gamma, \mu_1, \mu_2$ according to the typical values explained in Kribs-Zaleta and Mitchell (2014). Then, through solving (4) with the given values of the coefficients, we obtain measured values of the functions H, F, I as (7)–(9).

6.1 The direct problem

We first solve the direct problem (4), (5) with realistic data provided in Kribs-Zaleta and Mitchell (2014). The maximal number of eggs laid by the queen per day is set to $L = 2000$. As the eclosion function (1) suggests, this quantity is multiplied by the saturation function, where ω is the number of hive bees required for the emergence rate to reach $\frac{1}{2}L$. That fraction gives the proportion of eggs which survives to eclosion. We set $\omega = 15{,}000$ bees. In the recruitment rate (2) γ represents the healthy dynamics and it is set to $\gamma = \frac{1}{21}$, since in natural circumstances the hive bees are recruited in the forager class on the 21st day after eclosion. On the other hand, it takes a minimum of 7 days for a bee to mature enough to be able to forage, hence $\alpha = \frac{1}{7} - \frac{1}{21}$, which accounts for the unhealthy dynamics. φ, as ω, is a half saturation constant and it is the number of foragers at which the additional recruitment rate is $\frac{\alpha}{2}$. We set $\varphi = 1000$ bees. The infection rate (3) of susceptible bees is assumed to be $\beta = 0.8$ and the infection of plants to be $k = 100$. The «healthy» death occurs on the 21st day of foraging, so $\mu_1 = \frac{1}{21}$. An infected forager remains functional until emigrating or dying for 1.25 days in average, thus $\mu_1 = \frac{1}{1.25} = 0.8$. All rates are measured in units days^{-1}. The values satisfy the relation $L < \omega(\alpha + \gamma)$.

An extended foraging season from the end of the winter to the end of the summer is considered, which implies $T = 250$ days. We consider the healthy scenario first, that is $I^0 = 0$. We set $H^0 = 15{,}000$ and conduct experiments with two types of colonies, with and without presence of foragers in the beginning, $F^0 = 15{,}000$ or $F^0 = 0$. Following Algorithm 1, the results are plotted on Fig. 3.

It can be easily deduced that the colony is attracted to its disease-free equilibrium state regardless of the starting condition. At the initial time on Fig. 3 (right), it could be observed the accelerated recruitment which, however, do not lead to colony decline. In this case we are able to calculate the basic reproduction number (11) $\mathcal{R}_0 = 258.841 > 1$.

Now we perform a simulation of the unhealthy scenario. In this case we introduce $I^0 = 10$ infected bees at t_0. The experiments, again with $F^0 = 15{,}000$ and $F^0 = 0$ demonstrate the quick spread of the disease in the beginning, and then the colony tends to the same endemic equilibrium state (Fig. 4) thus the disease persists with the hive.

6.2 The inverse problem

Now we proceed to solve the inverse problem of identifying the parameter set $\boldsymbol{p} = (\alpha, \beta, \gamma, \mu_1, \mu_2)^\top = \left(\frac{2}{21}, 0.8, \frac{1}{21}, \frac{1}{21}, 0.8\right)^\top$ solving (4)–(6). We again let

Table 1 Simulation with $\boldsymbol{p}_0$ close to $\boldsymbol{p}$ and $\varepsilon_{\boldsymbol{p}} = 1e-6$

Parameter	p^i	p_0^i	$\check{p}^i$	$\lvert p^i - \check{p}^i \rvert$	$\frac{\lvert p^i - \check{p}^i \rvert}{p^i}$	r_0^i	$r_l^i,\ l \geq 1$
α	$\frac{2}{21}$	0.10	0.0952	1.7887e−6	1.8781e−5	7.3e−14	1e−15
β	0.8	0.75	0.8000	1.6155e−6	2.0193e−6	1e−14	1.9e−11
γ	$\frac{2}{21}$	0.05	0.0476	8.8612e−7	1.8608e−5	1.2e−14	9e−16
μ_1	$\frac{2}{21}$	0.05	0.0476	4.9691e−6	1.0435e−4	4.1e−13	8e−15
μ_2	0.8	0.75	0.8000	4.0667e−5	5.0834e−5	1e−14	1.99e−11

Table 2 Simulation with $\boldsymbol{p}_0$ far from $\boldsymbol{p}$ and $\varepsilon_{\boldsymbol{p}} = 2e-5$

Parameter	p^i	p_0^i	$\check{p}^i$	$\lvert p^i - \check{p}^i \rvert$	$\frac{\lvert p^i - \check{p}^i \rvert}{p^i}$	r_0^i	$r_l^i,\ l \geq 1$
α	$\frac{2}{21}$	0.5	0.0963	0.0011	0.0116	2.4e−9	8.1e−15
β	0.8	0.5	0.7996	3.5732e−4	4.4665e−4	5.3e−9	1e−14
γ	$\frac{2}{21}$	0.5	0.0474	2.4884e−4	0.0052	2.8e−10	1.5e−15
μ_1	$\frac{2}{21}$	0.5	0.0452	0.0025	0.0518	1e−10	5.3e−12
μ_2	0.8	0.5	0.7979	0.0021	0.0026	3.5e−8	1.1e−13

$L = 2000$, $\omega = 15{,}000$, $\varphi = 1000$, $k = 100$ and $t_0 = 0$, $T = 250$. We are going to simulate only the unhealthy scenario. This is because if no disease is involved, that is $I^0 = 0$, then from (4c) $\dot{I} = 0$ too and the values of β and μ_2 are undefined. We consider $H^0 = F^0 = 15{,}000$ and $I^0 = 10$.

Let us define 51 observations of type (7)–(9). We propose the following: during the first week, we suggest to perform 4 measurements per day, and then, from the $t = 13^{\text{th}}$ day, one measurement to be taken equidistantly for every 12 days. This is because the disease spreads very fast in the beginning, as we mentioned earlier.

Another interesting feature of the inverse problem is that we recover only rates. We set $\boldsymbol{p}_l \in \mathbb{S}_{\text{adm}} \equiv (0,1)^5\ \forall l$, see Algorithm 2. This makes the iteration procedure more 'fragile'. As a consequence, we have to tune the values of $\boldsymbol{r}_l$ (21), which cannot be the same for $l = 0$ and $l = 1, 2, \ldots$. As we show later, the values of $\boldsymbol{r}_l$ differ by orders of magnitude for different l. What is more, due to the ill-posedness of the inverse problem, it is hard to solve if the initial approximation $\boldsymbol{p}_0$ is too far from the true values of $\boldsymbol{p}$.

Now we present the solution to the inverse problem with an initial point $\boldsymbol{p}_0 = (0.1, 0.75, 0.05, 0.05, 0.75)^\top$, which is considered close to $\boldsymbol{p}$ (Table 1). It required 16 iterations for the procedure to converge.

The values of (12) are respectively $J_H(\check{\boldsymbol{p}}) = 0.0227$, $J_F(\check{\boldsymbol{p}}) = 0.0248$ and $J_I(\check{\boldsymbol{p}}) = 0.6205$. The experiments are done with $\varepsilon_{\boldsymbol{p}} = 1e-6$ and the values are pretty small which is a necessity condition for the parameters to be reconstructed accurately. What is more, the root mean squared errors are $\text{RMSE}_H(\check{\boldsymbol{p}}) = 0.0211$,

$\mathrm{RMSE}_F(\check{\boldsymbol{p}}) = 0.0221$ and $\mathrm{RMSE}_I(\check{\boldsymbol{p}}) = 0.1103$. It is approved by the negligible values of the absolute and the relative errors, see Table 1.

The next test is performed with an initial point $\boldsymbol{p}_0 = (0.5, 0.5, 0.5, 0.5, 0.5)^\top$, which is is interpreted as far from $\boldsymbol{p}$ (Table 2). Now 17 iterations are required for convergence, but we use $\varepsilon_{\boldsymbol{p}} = 2e-5$.

The values (12) in the 'far' case are respectively $J_H(\check{\boldsymbol{p}}) = 3.7105e+3$, $J_F(\check{\boldsymbol{p}}) = 3.5078e+3$ and $J_I(\check{\boldsymbol{p}}) = 8.0306e+3$. The numbers are so high, because they are calculated on $K = 51$ observations. The root mean squared errors are far smaller $\mathrm{RMSE}_H(\check{\boldsymbol{p}}) = 8.5297$, $\mathrm{RMSE}_F(\check{\boldsymbol{p}}) = 8.2934$ and $\mathrm{RMSE}_I(\check{\boldsymbol{p}}) = 12.5484$. Nevertheless, almost all relative parameter errors are around and below 1%, only the one associated with μ_1 is about 5%. For more accurate reconstruction, one has to set smaller $\varepsilon_{\boldsymbol{p}}$ and to process some more iterations.

We conclude the simulations conducting a test with perturbed observations to investigate the effect of measurement error on the parameter recovery. Let us consider the 'close' scenario and add a white noise to the observations (7)–(9). To say it more rigourously, a Gaussian noise is added to all data points such that the bias in a particular measurement is not greater than 1% with 95% confidence. We seed the random number generator for reproductivity of the results. The results are given in Table 3. We use $\varepsilon_{\boldsymbol{p}} = 1e-5$ and the same values of $\boldsymbol{r}_l$.

The values (12) of the cost functional are again relatively high: $J_H(\check{\boldsymbol{p}}) = 2.8587e+3$, $J_F(\check{\boldsymbol{p}}) = 349.8609$ and $J_I(\check{\boldsymbol{p}}) = 203.2855$. The difference in the components of $J(\check{\boldsymbol{p}})$ are explained by the difference in the magnitude of $H(t)$, on one hand, and $F(t)$ and $I(t)$ on the other hand. The root mean squared errors are again much smaller $\mathrm{RMSE}_H(\check{\boldsymbol{p}}) = 7.4869$, $\mathrm{RMSE}_F(\check{\boldsymbol{p}}) = 2.6192$ and $\mathrm{RMSE}_I(\check{\boldsymbol{p}}) = 1.9965$. All relative errors are less than 1e−3. The aggregated relative error, defined as $\mathrm{RE}_{\boldsymbol{p}} := \|\boldsymbol{p} - \check{\boldsymbol{p}}^{\mathrm{pert}}\|_\infty / \|\boldsymbol{p}\|_\infty$, is also small $\mathrm{RE}_{\boldsymbol{p}} = 9.5823e-4$, which implies the accuracy of the parameter reconstruction as well.

Generally, it could be implied that the Algorithm is very computationally efficient and it accurately identifies the parameters provided that the initial values are close to the real ones. The accuracy could be significantly improved if $\boldsymbol{r}_l$ are fine tuned for different $l = 1, 2, \ldots$ which, in turn, requires deep a priori investigation.

Table 3 Simulation with perturbed data and $\varepsilon_{\boldsymbol{p}} = 1e-5$

Parameter	p^i	p_0^i	$\check{p}^i$	$\lvert p^i - \check{p}^i \rvert$	$\dfrac{\lvert p^i - \check{p}^i \rvert}{p^i}$	r_0^i	$r_l^i,\ l \geq 1$
α	$\frac{2}{21}$	0.10	0.0952	4.7317e−5	4.9683e−4	7.3e−14	1e−15
β	0.8	0.75	0.8008	7.6732e−4	9.5914e−4	1e−14	1.9e−11
γ	$\frac{2}{21}$	0.05	0.0476	2.8269e−5	5.9365e−4	1.2e−14	9e−16
μ_1	$\frac{2}{21}$	0.05	0.0476	2.9668e−5	6.2303e−4	4.1e−13	8e−15
μ_2	0.8	0.75	0.8006	5.8557e−4	7.3196e−4	1e−14	1.99e−11

7 Conclusion

Recently there were observed ubiquitous massive losses of honeybee colonies, which should be paid attention to. The model we adopt does not shed light on what causes the CCD, but it demonstrates how the rapid decline happens and develops. The provided information might give an insight into how and to what extent the parameters influence the system behaviour, and in turn how to mitigate and eliminate the disorder's effect on a colony. It is crucial for the professional beekeepers to manage their apiaries in a way that prevents the colonies from pests, contagion, or another disease. The summarized qualitative analysis describes the interlinkage between the concepts of the bifurcation, the basic reproduction number and the Allee effect and how they interact to abruptly change the colony development, often leading to inevitable collapse.

The model itself is constituted by a system of three weakly coupled ODEs, where the dependent variables represent the population size of the hive bees, forage bees and infected foragers compartments. It considers both healthy and unhealthy dynamics, while accounting for disease transmission through mass action and interaction with plants. The tackled inverse problem in the paper focuses on recovering those parameters, which are determinative for the dynamics but are unobservable in practice. The adjoint state optimization approach is applied to solve the inverse problem, while the cost functional is minimized via a gradient method. The numerical simulations outline the algorithm properties, namely its ability to reconstruct the parameter values in accurate manner if provided with good initial approximation as well as its computational inexpensiveness.

The field of possible continuation and improvement of the research is spanless. A piece of effort is worth putting in investigation of more complex models that account for more details in dynamics and interaction with the surrounding environment, for instance modeling food store, mite and virus dynamics, seasonal patterns or taking the memory property into account via fractional-order derivatives. Future work might also include deeper qualitative analysis to provide better understanding of the sophisticated processed involved to restore failing apiaries and to suggest methodology for prevention of similar conditions, influencing nature, economics and industry.

Acknowledgements The authors are supported by the Bulgarian National Science Fund under Project KP-06-PN 46-7 "Design and research of fundamental technologies and methods for precision apiculture".

References

Abdulla UG, Poteau R (2021) Identification of parameters for large-scale kinetic models. J Comput Phys 429:110026

Amdam GV, Omholt SW (2003) The hive bee to forager transition in honeybee colonies: the double repressor hypothesis. J Theor Biol 223(4):451–464

Atanasov AZ, Georgiev SG, Vulkov LG (2021) Parameter identification of colony collapse disorder in honeybees as a contagion. Commun Comput Inf Sci 1341:363–377

Bagheri S, Mirzaie M (2019) A mathematical model of honey bee colony dynamics to predict the effect of pollen on colony failure. PLoS ONE 14(11):e0225632

Bailey L (2002) The Isle of Wight Desease. Central Association of Bee-Keepers

Becher MA, Osborne JL, Thorbek P, Kennedy PJ, Grimm V (2013) Review: towards a systems approach for understanding honeybee decline: a stocktaking and synthesis of existing models. J Appl Ecol 50:868–880

Berenguer MI, Kunze H, La Torre D, Ruiz Galán M (2016) Galerkin method for constrained variational equations and a collage-based approach to related inverse problems. J Comp Appl Math 292:67–75

Booton RD, Iwasa Y, Marshall JAR, Childs DZ (2017) Stress-mediated Allee effects can cause the sudden collapse of honey bee colonies. J Theor Biol 420:213–219

Chowell G, Brauer F (2009) The basic reproduction number of infectious diseases: computation and estimation using compartmental epidemic models. In Chowell G, Hayman JM, Bettencourt LMA, Castillo-Chavez C (Eds) Mathematical and statistical estimation approaches in epidemiology. Springer, Dordrecht, pp 1–30

Cox-Foster DL, Conlan S, Holmes EC, Palacios G, Evans JD, Moran NA, Quan P-L, Briese T, Hornig M, Geiser DM, Martinson V, vanEngelsdorp D, Kalkstein AL, Drysdale A, Hui J, Zhai J, Cui L, Hutchison SK, Simons JF, Egholm M, Pettis JS, Lipkin WI (2007) A metagenomic survey of microbes in honey bee Colony Collapse Disorder. Sci 318:283–287

Dornberger L, Mitchell C, Hull B, Ventura W, Shopp H, Kribs-Zaleta C, Kojouharov H, Grover J (2012) Death of the bees: a mathematical model of Colony Collapse Disorder. Technical Report 2012-12, Mathematics Preprint Series, University of Texas at Arlington Mathematics Department

Ellis JD, Evans JD, Pettis J (2010) Colony losses, managed colony population decline, and Colony Collapse Disorder in the United States. J Apic Res 49(1):134–136

Fact Sheet (2015) The economic challange posed by declining pollinator populations. Office the Press Secretary, The White House

Finley J, Camazine S, Frazier M (1996) The epidemic of honey bee colony losses during the 1995–1996 season. Am Bee J 136:805–808

Khoury DS, Myerscough MR, Barron AB (2011) A quantitative model of honey bee colony population dynamics. PLoS ONE 6(4):e18491

Khoury DS, Barron AB, Meyerscough MR (2013) Modelling food and population dynamics honey bee colonies. PLoS ONE 8(5):e0059084

Kralj J, Fuchs S (2006) Parasitic mites influence flight duration and homing ability of infested Apis mellifera foragers. Apidologie 37:577–587

Kribs-Zaleta CM, Mitchell C (2014) Modeling Colony Collapse Disorder in honeybees as a contagion. Math Biol Eng 11(6):1275–1294

Kulincevic JM, Rothenbuhler WC, Rinderer TE (1982) Disappearing disease. Part 1—effects of certain protein sources given to honey bee colonies in Florida. Am Bee J 122:191–198

Kunze HE, Vrscay ER (1999) Solving inverse problems for ordinary differential equations using the Picard contraction mapping. Inv Probl 15:745–770

Kunze HE, Hicken JE, Vrscay ER (2004) Inverse problems for ODEs using contraction maps and suboptimality of the 'collage method'. Inv Probl 20(3):977–991

Kunze HE, La Torre D, Vrscay ER (2009) A generalized collage method based upon the Lax–Milgram functional for solving boundary value inverse problems. Nonlinear Anal 71:e1337–e1343

Kunze HE, La Torre D, Mendivil F, Ruiz Galán M, Zaki R (2014) Fractal-based methods and inverse problems for differential equations: current state of the art. Math Probl Eng 2014:737694

Kunze HE, La Torre D, Levere K, Ruiz Galán M (2015) Inverse problems via the "Generalized collage theorem" for vector-valued Lax–Milgram-based variational problems. Math Probl Eng 2015:764643

Ma C, Jiang L (2007) Some research on Levenberg–Marquardt method for the nonlinear equations. Appl Math Comput 184(2):1032–1040

Ma Z, Zhou Y, Wu J (2009) Modeling and dynamics of infectious diseases. World Scientific Publishers, Singapore

Marchuk GI (1995) Adjoint equations and analysis of complex systems. Kluwer, Dordrecht

Marchuk GI, Agoshkov VI, Shutyaev VP (1996) Adjoint equations and perturbation algorithms in nonlinear problems. CRC Press, Boca Raton

Oldroyd BP (2007) What's killing american honey bees? PLoS Biol 5(6):e168 1195–1199

Paxton RJ (2010) Does infection by Nosema ceranae cause "Colony Collapse Disorder" in honey bees (Apis mellifera)? J Apic Res 49(1):80–84

Ratti V, Kevan PG, Eberl HJ (2017) A mathematical model of forager loss in honeybee colonies infested with Varroa destructor and the acute bee paralysis virus. Bull Math Biol 79(6):1218–1253

Russel S, Barron AB, Harris D (2013) Dynamics modelling of honeybee (Apis mellifera) colony growth and failure. Ecol Model 265:138–169

Silver J (1907) The isle of Wight bee-disease. Br Bee J 35:223–224

Switanek M, Crailsheim K, Truhetz H, Brodschneider R (2017) Modelling seasonal effects of temperature and precipitation on honey bee winter mortality in a temperate climate. Sci Tot Environ 579:1581–1587

Torres DJ, Ricoy VM, Roybal S (2015) Modelling honey bee populations. PLoS ONE 10(7):e0130966

Usaini S, Lloyd AL, Anguelov R, Garba SM (2017) Dynamical behavior of an epidemiological model with a demographic Allee effect. Math Comput Simul 133:311–325

van der Zee R, Pisa L, Andronov S, Brodschneider R, Charriere JD, Chlebo R, Coffey MF, Cralisheim K, Dahle B, Gajda A et al (2012) Managed honey bee colony losses in Canada, China, Europe, Israel and Turkey for the winters of 2008–2009 and 2009–2010. J Apic Res 51(1):100–114

vanEngelsdorp D, Evans JD, Saegerman C, Mullin C, Haubruge E, Nguyen BK, Frazier M, Frazier J, Cox-Foster D, Chen Y, Underwood R, Tarpy DR, Pettis JS (2009) Colony collapse disorder: a descriptive study. PLoS ONE 4(8):e6381

Winston WL (1991) The biology of the honey bee. Harvard University Press, Cambridge Mass

Yıldız TA (2018) A fractional dynamical model for honeybee colony population. Int J Biomath 11(5):1850063